Topological Quantum State Control through Exceptional-Point Proximity

Maryam Abbasi, Weijian Chen, Mahdi Naghiloo, Yogesh N. Joglekar, and Kater W. Murch

Topological quantum state control through exceptional-point proximity

Maryam Abbasi,[1] Weijian Chen,[1, 2] Mahdi Naghiloo,[1, 3] Yogesh N. Joglekar,[4, *] and Kater W. Murch[1, 2, †]

[1]*Department of Physics, Washington University, St. Louis, Missouri 63130*
[2]*Center for Quantum Sensors, Washington University, St. Louis, Missouri 63130*
[3]*Research Laboratory of Electronics, MIT, Cambridge, Massachusetts 02139*
[4]*Department of Physics, Indiana University Purdue University Indianapolis (IUPUI), Indianapolis, Indiana 46202*
(Dated: March 17, 2022)

We study the quantum evolution of a non-Hermitian qubit realized as a submanifold of a dissipative superconducting transmon circuit. Real-time tuning of the system parameters to encircle an exceptional point results in non-reciprocal quantum state transfer. We further observe chiral geometric phases accumulated under state transport, verifying the quantum coherent nature of the evolution in the complex energy landscape and distinguishing between coherent and incoherent effects associated with exceptional point encircling. Our work demonstrates an entirely new method for control over quantum state vectors, highlighting new facets of quantum bath engineering enabled through dynamical non-Hermitian control.

Small quantum systems that interact with an environment can be described by a Lindblad density matrix equation that encodes their approach to steady state. When the quantum trajectories of these decoherence-inducing dynamics are restricted to those with no quantum jumps, the resulting evolution is described by an effective non-Hermitian Hamiltonian. Such non-Hermitian quantum systems have complex energies, non-orthogonal eigenstates, and undergo a coherent, non-unitary evolution. The presence of special kinds of degeneracies known as exceptional points (EPs) play an important role in the unique characteristics of these non-Hermitian systems [1, 2]. Such EPs occur when both the eigenvalues and eigenstates of the system coalesce. A plethora of phenomena associated with EPs have been revealed in classical platforms such as mechanical and optical systems [3–9]. In the vicinity of the EP, the shape of the Riemann manifold that describes the complex energies of a non-Hermitian system can lead to fundamentally new phenomena that are not present in their Hermitian counterparts with strictly real energies. For a second-order EP degeneracy, quasi-static tuning of the Hamiltonian parameters is expected to map one eigenstate, $|\psi_-\rangle$, to the other $e^{i\chi_+}|\psi_+\rangle$, modulo a global phase χ_+. Furthermore, the geometric part of the global phase is expected to be chiral [10–15]. Such mode-switch behavior has been demonstrated in classical systems [16–19], yet the extension of such topological control to quantum systems—with no classical counterpart—has remained an outstanding goal in the field [20].

Here, we utilize the quantum energy levels of a superconducting circuit described by an effective non-Hermitian Hamiltonian to study quantum state control in the vicinity of the system's EPs. While our previous work [21] characterized the static properties of this non-Hermitian system, we now employ dynamical control of the Hamiltonian parameters and observe chiral quantum state transfer when encircling EPs. We further use an auxiliary level of our quantum circuit to verify the coherent nature of this evolution and examine the geometric phases accumulated from quantum state transport. These reveal that a π phase difference associated with the chirality of the transport persists under non-Hermitian dynamical quantum evolution. Finally, we exploit state transfer in the limit of fast, closed-loop parameter variation, which goes beyond the slow driving limit demonstrated in previous works [16–19] and reveals a broad parameter range proximity to EPs for successful state transfer.

Our experiment comprises a superconducting Transmon circuit [22, 23] embedded inside a three-dimensional copper cavity (Fig. 1a) [24]. The circuit has anharmonic energy states and the first four energy levels are labeled by $|g\rangle, |e\rangle, |f\rangle$, and $|h\rangle$. The cavity mediates interaction with an environment that is set by the density of states in a microwave transmission line. We shape this density of states to enhance the dissipation of the $|e\rangle$ state while suppressing dissipation of the $|f\rangle$ state. While the evolution of the four-level quantum system can be described by a Lindblad equation, the evolution within the excited (and lossy) manifold of states $\{|e\rangle, |f\rangle\}$ can be described by an effective non-Hermitian Hamiltonian [21, 25].

By introducing a microwave drive with detuning $\Delta = \omega_{ef} - \omega_d$, where ω_{ef} is the transition frequency between the $|e\rangle$ and $|f\rangle$ states, and ω_d is the microwave drive frequency, we produce the effective Hamiltonian in the frame rotating with the drive:

$$H_{\text{eff}}/\hbar = J(|e\rangle\langle f| + |f\rangle\langle e|) + (\Delta - i\gamma/2)|e\rangle\langle e| \quad (1)$$

where J is the coupling rate between $|e\rangle$ and $|f\rangle$, and γ is the decay rate of the $|e\rangle$ state. Quantum dynamics of the qubit are given by the (complex) eigenvalues $\lambda_\pm$ and (non-orthogonal) eigenstates $|\psi_\pm\rangle$ of the Hamiltonian (expressed in the energy basis);

$$\lambda_\pm = \Delta/2 - i\gamma/4 \pm \sqrt{J^2 + (\Delta/2 - i\gamma/4)^2}, \quad (2)$$

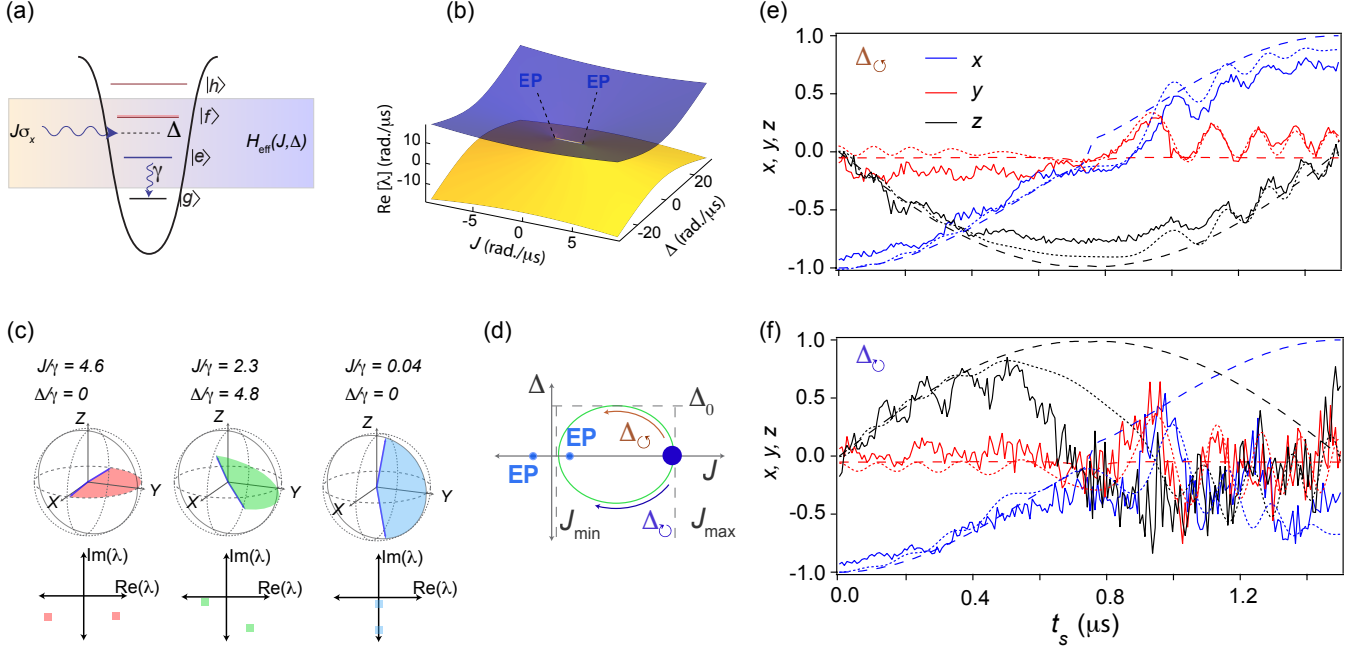$$|\psi_\pm\rangle \propto \begin{pmatrix} \lambda_\pm \\ J \end{pmatrix}. \quad (3)$$

FIG. 1: **Dynamically encircling an EP.** (a), The energy states of the transmon circuit with the non-Hermitian qubit submanifold $\{|e\rangle, |f\rangle\}$ highlighted. The Hamiltonian parameters J and Δ are tuned with a microwave drive. (b), In the static limit, the eigenenergies are described by Riemann manifolds. (c), The eigenstates and eigenvalues of H_{eff} are indicated for different values of J and Δ. The colored planes indicate the opening angle between the two eigenstates for clarity. (d), The parameter sweeps are designated by direction ($\Delta_\circlearrowright$, $\Delta_\circlearrowleft$) and J_{min}. (e,f), Quantum state tomography (solid lines, expressed as the Pauli expectation values x, y, z) reveals the state evolution along the parameter path for the $\Delta_\circlearrowright$ ($\Delta_\circlearrowleft$) direction. The long-dashed lines indicate the instantaneous eigenstates of H_{eff} and the fine-dashed lines are the solution to the Lindblad equation [24].

The real part of eigenenergies in the parameter space (J, Δ) is provided in Fig. 1b, and the eigenstates for select values of J and Δ are sketched in Fig. 1c. The static EP degeneracies occur at $J_{\mathrm{EP}} = \pm\gamma/4$.

Quantum state tomography [26] allows us to study the state of the qubit as the parameters of the Hamiltonian are tuned in real time. We study a parameter loop specified by initial/final parameters $\Delta = 0$ and $J_{\mathrm{max}} = 30$ rad/μs and the parameter variation; $\Delta(t) = \Delta_{\circlearrowright,\circlearrowleft} \sin(2\pi t/T)$ and $J(t) = (J_{\mathrm{max}} - J_{\mathrm{min}}) \cos^2(\pi t/T) + J_{\mathrm{min}}$ (Fig. 1d). The sign of $\Delta_{\circlearrowright,\circlearrowleft}$ determines whether the sweep is counterclockwise or clockwise, and the sign of J is determined by the phase of the drive. Tomography along the path is achieved by dividing the time evolution into sequentially longer steps $t_{\mathrm{s}} \in [0, T]$, pausing the evolution at t_{s} and performing measurements to determine Pauli expectation values $x \equiv \langle\sigma_x\rangle$, $y \equiv \langle\sigma_y\rangle$ and $z \equiv \langle\sigma_z\rangle$ in the energy basis of the $\{|e\rangle, |f\rangle\}$ qubit.

We slowly vary the system parameters in a loop given by $T = 1.5$ μs and $J_{\mathrm{min}} = 0.3$ rad/μs. By choosing $\Delta_\circlearrowright = 10\pi$ rad/μs (Fig. 1e), the system evolves from ρ_-, where $\mathrm{tr}(\rho_- \sigma_x) \simeq -1$, roughly following the instantaneous eigenstates of H_{eff}. After a complete loop that encircles the EP, the system does not return to the initial state, instead the final state is close to ρ_+ which

is nearly orthogonal to the initial state. This observation can be qualitatively understood by walking through the Riemann structure associated with the static EP; the qubit follows the Riemann surface crossing onto the upper sheet at the branch cut connecting the two EPs (Fig. 1b). In addition, finite time evolution induces transitions between the two eigenstates of the system, leading to a small oscillation in the Pauli expectation values, with frequency given by the real part of the energy difference of the eigenstates. These oscillations are in reasonable agreement with the solution to the Lindblad equation [24].

In contrast, if we choose $\Delta_\circlearrowleft = -10\pi$ rad/μs, corresponding to encircling the static EP in a clockwise direction, the system does not evolve along the instantaneous eigenstates. As shown in Fig. 1f, the state significantly deviates from the eigenstate in the vicinity of the EP. This can be attributed to non-Hermitian gain/loss effects observed in previous works [16–19] as well as other sources of dissipation [27, 28]. Along this parameter path, the imaginary component of the eigenenergy corresponds to larger loss, resulting in a reduced postselection probability as can be seen in the increased noise in the data. In the postselected manifold the loss of one eigenstate can be viewed as a relative gain of the other eigen-
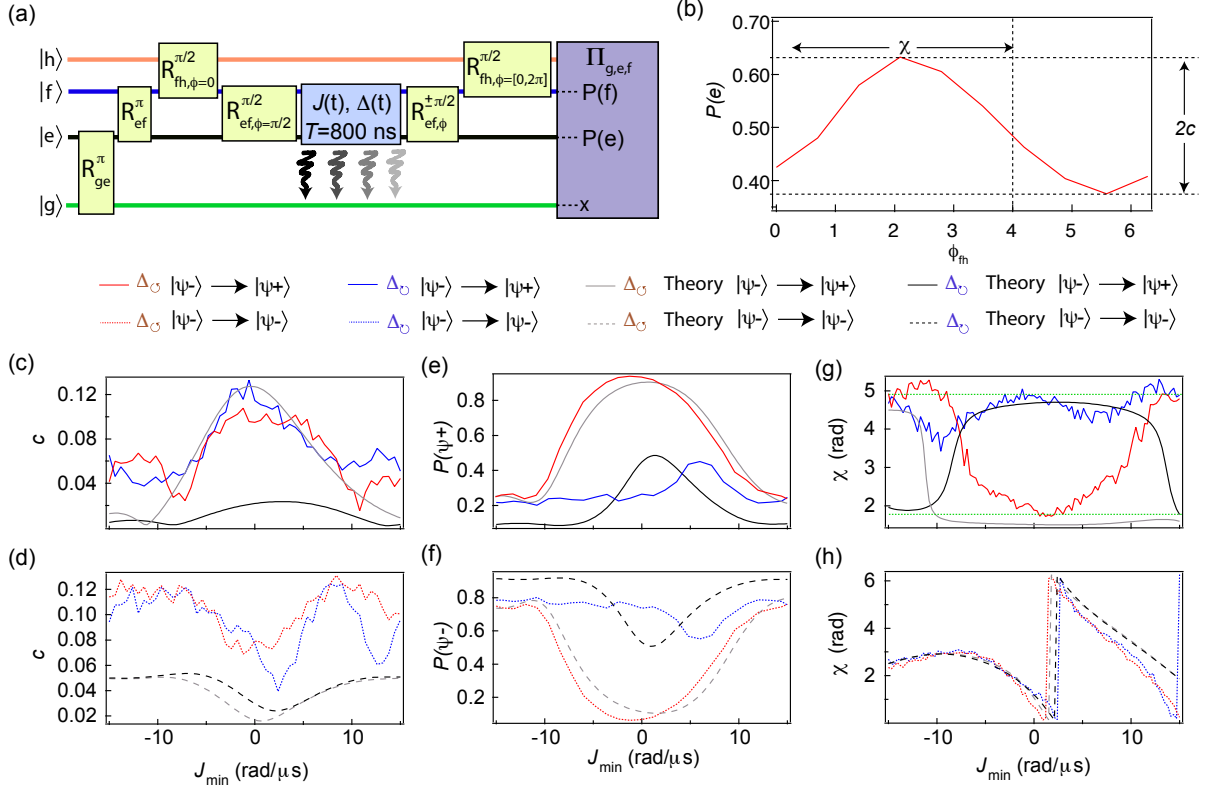
FIG. 2: **Coherent state transport and geometric phase measurement**. (a), Experiment schematic; a series of resonant rotations prepare a superposion between the state $|\psi_-\rangle$ and state $|h\rangle$. The $|h\rangle$ state is used as a quantum phase reference to determine the accumulated phase on the quantum states that evolve in the non-Hermitian Floquet Hamiltonian. After evolution for $T = 800$ ns, the rotation $R_{ef}^{\pm\pi/2}$ determines which qubit state ($|\psi_+\rangle$ or $|\psi_-\rangle$) is interfered with the $|h\rangle$ reference. (b), By sweeping the phase of the final $R_{fh}^{\pi/2}$ rotation we determine the contrast c and phase χ. The interference contrast (c,d) and state populations (e,f) of final states $|\psi_\pm\rangle$ for $\Delta_\circlearrowleft$ and $\Delta_\circlearrowright$ sweep directions. (g, h), Extracted total phases; the dashed green lines indicate a phase difference of π. The associated gray and black curves indicate the result from the Lindblad equation simulation.

state. Any small fraction of population that is seeded by non-adiabaticity or dissipation into the relative gain eigenstate is therefore amplified. This gain/loss effect does not occur for the $\Delta_\circlearrowleft$ sweep because the system follows the instantaneous eigenstate with relative gain which is stable against non-adiabaticity and dissipation.

In order to investigate the quantum nature of *state* transport, as opposed to the transfer of *population* between eigenstates [16–19], we make use of the $|h\rangle$ level as a quantum phase reference, as shown in Fig. 2a. Resonant rotations are used to initialize the three-state system in the state $\rho \propto (|h\rangle + |\psi_-\rangle)(\langle h| + \langle \psi_-|)$. The qubit then undergoes dynamical evolution under the time-dependent Hamiltonian specified by $J_{\min}$, $\Delta_{\circlearrowright,\circlearrowleft} = \pm 10\pi$ rad/μs, and for $T = 800$ ns. After this evolution, the three-state system is in general in a mixed state, $\rho \propto c_-(|h\rangle + e^{i\chi_-}|\psi_-\rangle)(\langle h| + e^{-i\chi_-}\langle\psi_-|) + c_+(|h\rangle + e^{i\chi_+}|\psi_+\rangle)(\langle h| + e^{-i\chi_+}\langle\psi_+|)$ involving both qubit eigenstates, where $\chi_\pm$ are phases accumulated on the states.

We note that coherent terms such as $|\psi_-\rangle\langle\psi_+|$ remain negligible during the evolution. A second rotation is used to rotate either the $|\psi_+\rangle$ or $|\psi_-\rangle$ into the state $|f\rangle$ which then interferes with the $|h\rangle$ reference. We determine the contrast c and total phase χ from the resulting interference (Fig. 2b).

In Figure 2c and d, we display the measured contrast for the $|\psi_+\rangle$ and $|\psi_-\rangle$ final states. In the vicinity of $J_{\min} = 0$, we observe higher contrast for the $|\psi_+\rangle$ final state for both the $\Delta_\circlearrowright$ and $\Delta_\circlearrowleft$ parameter sweeps, indicating that the state transport ($|\psi_\mp\rangle \rightarrow e^{i\chi_\pm}|\psi_\pm\rangle$) is quantum coherent. In comparison, we display in Fig. 2d and e the populations of the two states for the two directions. Near $J_{\min} = 0$, our observation of larger populations in the $|\psi_+\rangle(|\psi_-\rangle)$ states for $\Delta_\circlearrowright(\Delta_\circlearrowleft)$ sweeps (Fig. 2e, red solid and Fig. 2f, blue dashed) is consistent with "chiral" features associated nonreciprocal population/energy transfer observed in previous work [16–19]. Here relative gain/loss of the two paths favors one or the other final states. This chiral effect, however, is com-

paratively incoherent, showing reduced contrast despite larger population. Whereas the gain/loss effects arising from the imaginary energy components can favor population transfer between states, this process is not necessarily coherent. The interference contrast therefore distinguishes between coherent state transport and incoherent population transfer between states.

We now examine the total quantum phases accumulated for the two encircling directions, as displayed in Fig. 2g,h. In general, the total quantum phase will be the sum of a dynamical phase arising from Hamiltonian evolution and a geometric phase. This is apparent in Fig. 2h where we observe significant dependence of the phase on the sweep parameter J_{min}. However, for state transport that follows the Riemann surfaces, we expect the dynamical phase to cancel as the state spends equal time in either energy eigenstate. This results in the relative insensitivity of the total phase to the sweep parameter as shown in Fig. 2g. Here we observe a π phase difference between the $\Delta_{\circlearrowleft}$ and $\Delta_{\circlearrowright}$ sweeps as is anticipated from the static structure of EPs [10–15]. Qualitatively, this π phase difference arises because one path passes through the excited state of the qubit, while the other does not.

While the quantum state transfer under quasistatic tuning of the system parameters is best understood as a walk through the complex-energy landscape of a static Hamiltonian H_{eff} with EPs (Fig. 1b), our results in Fig. 2d clearly indicate that in the dynamical case the state transfer can happen in a broad range of the parameter J_{min} that includes the situations of encircling zero, one, and two EPs. We attribute this observation to the non-adiabatic coupling near the EPs, which occurs when the parameter sweeps are not infinitely slow [29].

To further investigate the nature of state transfer beyond the slow driving limit, as is relevant in any real-time operation on quantum states, we now study the population transfer in the limit of fast parameter variation. As before, we prepare the system in the state $\rho_- \simeq |\psi_-\rangle\langle\psi_-|$ and perform closed loop parameter variation for different loop periods T and J_{min}. After one complete encircling (at time $t = T$) we use quantum state tomography to determine $P(\psi_-)$, the population in $|\psi_-\rangle$ as displayed in Fig. 3. We consider both $\Delta_{\circlearrowleft}$ (Fig. 3a) and $\Delta_{\circlearrowright}$ (Fig. 3b) directions. We observe a rich dependence on the parameters of the loop, which is qualitatively reproduced by the corresponding Lindblad simulations [24] as shown in Fig. 3c,d. Figure 3e displays a linecut of $P(\psi_-)$ showing the dependence of $P(\psi_-)$ on the loop duration. These observations indicate that successful quantum state transfer can occur in the fast driving limit.

Our investigation of state transport in the vicinity of exceptional point degeneracies reveals new methods of quantum coherent state control of dissipative systems enabled through non-Hermitian Hamiltonian dynamics. This work, and the robustness with which we observe the predicted chiral geometric phases, opens new av-
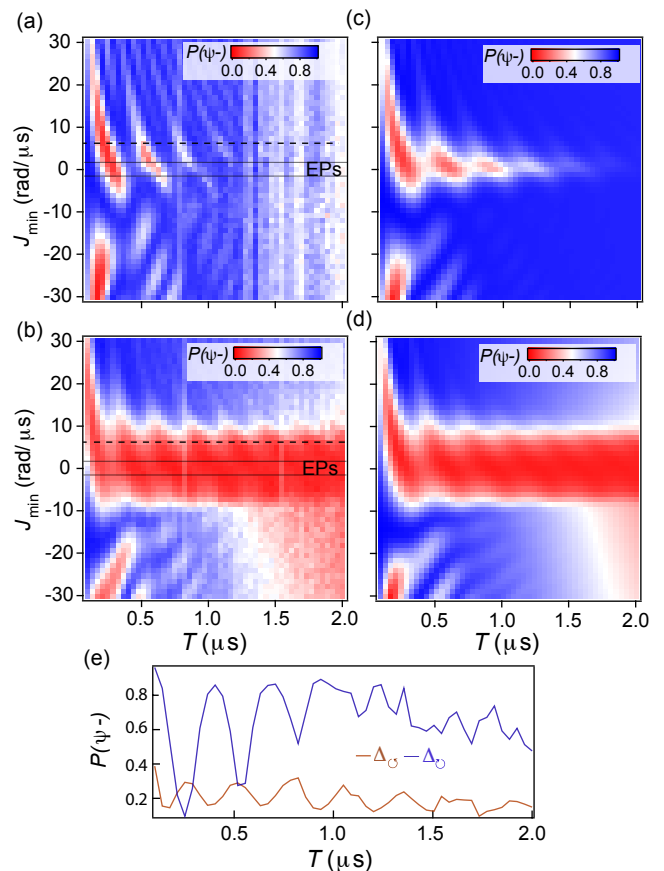

FIG. 3: **Population transfer beyond slow-driving limit.** (a,b), The eigenstate population $P(\psi_-)$ after one period evolution for the two sweep directions $\Delta_{\circlearrowleft}$ and $\Delta_{\circlearrowright}$ are displayed versus J_{min} and T. Black solid lines indicate the location of second-order static EPs. (c,d), Corresponding simulation results for the two sweep directions. (e), Two cuts from panels (a) [(b)] shown in blue (red) at $J_{min} = 6$ rad/μs. The locations of the line cuts are indicated as dashed lines in (a,b).

enues to investigations of eigenvalue braiding in larger dimension non-Hermitian systems [30, 31], allowing the study of exotic topological classes of these (knotted) systems. Future extensions to non-Hermiticities through non-reciprocity [32] would enable scaling to quantum many-body systems where the study of topological edge-states and invariants [33, 34] are expected to yield deviations from the paradigmatic bulk-boundary correspondence [35, 36]. Finally, the interplay of quantum measurement dynamics [37–39] with the non-Hermitian dynamics explored here is expected to produce new fruitful avenues for quantum control.

———————

* yojoglek@iupui.edu

† murch@physics.wustl.edu

[1] Özdemir, Ş. K., Rotter, S., Nori, F. & Yang, L. Parity–time symmetry and exceptional points in photonics. *Nature Materials* **18**, 783–798 (2019).

[2] Miri, M.-A. & Alù, A. Exceptional points in optics and photonics. *Science* **363**, eaar7709 (2019).

[3] Guo, A. *et al.* Observation of $\mathcal{PT}$-Symmetry Breaking in Complex Optical Potentials. *Phys. Rev. Lett.* **103**, 093902 (2009).

[4] Rüter, C. E. *et al.* Observation of parity—time symmetry in optics. *Nature physics* **6**, 192 (2010).

[5] Peng, B. *et al.* Parity-time-symmetric whispering-gallery microcavities. *Nature Physics* **10**, 394–398 (2014).

[6] Hodaei, H., Miri, M.-A., Heinrich, M., Christodoulides, D. N. & Khajavikhan, M. Parity-time-symmetric microring lasers. *Science* **346**, 975–978 (2014).

[7] Zeuner, J. M. *et al.* Observation of a Topological Transition in the Bulk of a Non-Hermitian System. *Phys. Rev. Lett.* **115**, 040402 (2015).

[8] Li, J. *et al.* Observation of parity-time symmetry breaking transitions in a dissipative Floquet system of ultracold atoms. *Nature Communications* **10**, 855 (2019).

[9] Xiao, L. *et al.* Observation of topological edge states in parity-time-symmetric quantum walks. *Nature Physics* **13**, 1117–1123 (2017).

[10] Dembowski, C. *et al.* Experimental Observation of the Topological Structure of Exceptional Points. *Phys. Rev. Lett.* **86**, 787–790 (2001).

[11] Dembowski, C. *et al.* Encircling an exceptional point. *Physical Review E* **69**, 056216 (2004).

[12] Gao, T. *et al.* Observation of non-Hermitian degeneracies in a chaotic exciton-polariton billiard. *Nature* **526**, 554–558 (2015).

[13] Heiss, W. Phases of wave functions and level repulsion. *The European Physical Journal D - Atomic, Molecular and Optical Physics* **7**, 1–4 (1999).

[14] Mailybaev, A. A., Kirillov, O. N. & Seyranian, A. P. Geometric phase around exceptional points. *Physical Review A* **72**, 014104 (2005).

[15] Mehri-Dehnavi, H. & Mostafazadeh, A. Geometric phase for non-Hermitian Hamiltonians and its holonomy interpretation. *Journal of Mathematical Physics* **49**, 082105 (2008).

[16] Xu, H., Mason, D., Jiang, L. & Harris, J. G. E. Topological energy transfer in an optomechanical system with exceptional points. *Nature* **537**, 80–83 (2016).

[17] Doppler, J. *et al.* Dynamically encircling an exceptional point for asymmetric mode switching. *Nature* **537**, 76–79 (2016).

[18] Yoon, J. W. *et al.* Time-asymmetric loop around an exceptional point over the full optical communications band. *Nature* **562**, 86–90 (2018).

[19] Zhang, X.-L., Wang, S., Hou, B. & Chan, C. Dynamically Encircling Exceptional Points: In situ Control of Encircling Loops and the Role of the Starting Point. *Physical Review X* **8**, 021066 (2018).

[20] Liu, W., Wu, Y., Duan, C.-K., Rong, X. & Du, J. Dynamically Encircling an Exceptional Point in a Real Quantum System. *Phys. Rev. Lett.* **126**, 170506 (2021).

[21] Naghiloo, M., Abbasi, M., Joglekar, Y. N. & Murch, K. W. Quantum state tomography across the exceptional point in a single dissipative qubit. *Nature Physics* **15**, 1232–1236 (2019).

[22] Koch, J. *et al.* Charge-insensitive qubit design derived from the Cooper pair box. *Phys. Rev. A* **76**, 042319 (2007).

[23] Paik, H. *et al.* Observation of High Coherence in Josephson Junction Qubits Measured in a Three-Dimensional Circuit QED Architecture. *Phys. Rev. Lett.* **107**, 240501 (2011).

[24] Supplemental information contains further details regarding the setup, methods, and theoretical modeling.

[25] Mølmer, K., Castin, Y. & Dalibard, J. Monte Carlo wavefunction method in quantum optics. *Journal of the Optical Society of America B* **10**, 524 (1993).

[26] Steffen, M. *et al.* Measurement of the Entanglement of Two Superconducting Qubits via State Tomography. *Science* **313**, 1423–1425 (2006).

[27] Minganti, F., Miranowicz, A., Chhajlany, R. W. & Nori, F. Quantum exceptional points of non-Hermitian Hamiltonians and Liouvillians: The effects of quantum jumps. *Phys. Rev. A* **100**, 062131 (2019).

[28] Chen, W., Abbasi, M., Joglekar, Y. N. & Murch, K. W. Quantum Jumps in the Non-Hermitian Dynamics of a Superconducting Qubit. *Phys. Rev. Lett.* **127**, 140504 (2021).

[29] Hassan, A. U. *et al.* Chiral state conversion without encircling an exceptional point. *Physical Review A* **96** (2017).

[30] Carlström, J., Stålhammar, M., Budich, J. C. & Bergholtz, E. J. Knotted non-Hermitian metals. *Phys. Rev. B* **99**, 161115 (2019).

[31] Höller, J., Read, N. & Harris, J. G. E. Non-Hermitian adiabatic transport in spaces of exceptional points. *Phys. Rev. A* **102**, 032216 (2020).

[32] Wang, Y.-X. & Clerk, A. A. Non-Hermitian dynamics without dissipation in quantum systems. *Phys. Rev. A* **99**, 063834 (2019).

[33] Yao, S. & Wang, Z. Edge States and Topological Invariants of Non-Hermitian Systems. *Phys. Rev. Lett.* **121**, 086803 (2018).

[34] Kunst, F. K., Edvardsson, E., Budich, J. C. & Bergholtz, E. J. Biorthogonal Bulk-Boundary Correspondence in Non-Hermitian Systems. *Phys. Rev. Lett.* **121**, 026808 (2018).

[35] Weidemann, S. *et al.* Topological funneling of light. *Science* **368**, 311–314 (2020).

[36] Xiao, L. *et al.* Non-Hermitian bulk–boundary correspondence in quantum dynamics. *Nature Physics* **16**, 761–766 (2020).

[37] Weber, S. J. *et al.* Mapping the optimal route between two quantum states. *Nature* **511**, 570–573 (2014).

[38] Minev, Z. K. *et al.* To catch and reverse a quantum jump mid-flight. *Nature* **570**, 200–204 (2019).

[39] Van Regemortel, M., Cian, Z.-P., Seif, A., Dehghani, H. & Hafezi, M. Entanglement Entropy Scaling Transition under Competing Monitoring Protocols. *Phys. Rev. Lett.*

126, 123604 (2021).

[40] Wallraff, A. *et al.* Approaching Unit Visibility for Control of a Superconducting Qubit with Dispersive Readout. *Phys. Rev. Lett.* **95**, 060501 (2005).

[41] Hatridge, M., Vijay, R., Slichter, D. H., Clarke, J. & Siddiqi, I. Dispersive magnetometry with a quantum limited SQUID parametric amplifier. *Phys. Rev. B* **83**, 134501 (2011).

[42] Castellanos-Beltran, M. A., Irwin, K. D., Hilton, G. C., Vale, L. R. & Lehnert, K. W. Amplification and squeezing of quantum noise with a tunable Josephson metamaterial. *Nature Physics* **4**, 929–931 (2008).